DARPA-HR0011-16-1-0006, Superior AI Phase 2
Quarterly Report Q1, 9/12/2017 – 12/31/2017

Supplementary Technical Report Task 1:
Energy-Aware Computing for Improved Energy Utilization

Abstract

In mainstream AI methods, energy efficiency usually has not been considered as a key constraint; rather many AI solutions use "brute force" and require huge amount of computing power to achieve the desired performance. Studying efficient energy consumption in brain's intelligence helps us to design AI that is energy efficient. We develop superior AI in which energy constraint leads to intelligence. In our working model, spiking neuron populations are combined with metabolic equations in a unique way. One salient point of our model is the coupling of physiological processes at a broad range of time scales with many orders of magnitude differences: (1) fast neuron spiking at milliseconds scale; (2) metabolic processes at a time scale of fractions of a second; (3) and vascular effects of blood flow (energy supply) at much smaller time scales of 10s or more. We compare and explore specific advantages of these approaches when studying intermittent synchronization effects as hallmarks of the brain's intelligent functions.

1. Introduction

As computers, smartphones, and communication networks become more powerful computationally, they also require more power to run. While it is tempting to think that the power consumption of digital devices diminish *pari passu* with smaller integrated circuit (IC) fabrication technology, or even surpass it, this is not the case. For example, even though the process feature size of IC components has been shrinking exponentially over the past several decades in according with Moore's law, the actual power consumption raises exponentially (SIA, 2015; see figure 1).

Attempts by engineers to curtail the energy consumption of digital devices in step with increasing computational power of these devices has had mixed results. Again, as described above, the miniaturization process has been the best friend of the CMOS logic-gate designer as the power consumption per gate reduces precipitously with shrinking process feature size. However, this gift has its limits, as described above. Some other methods that engineers are using to make up the slack include techniques such as "power gating," which shuts off blocks of the IC that are not currently in use (Roy et al. 2003), and "dual-voltage CPUs," which vary the voltage between the processor core and input/output operations.
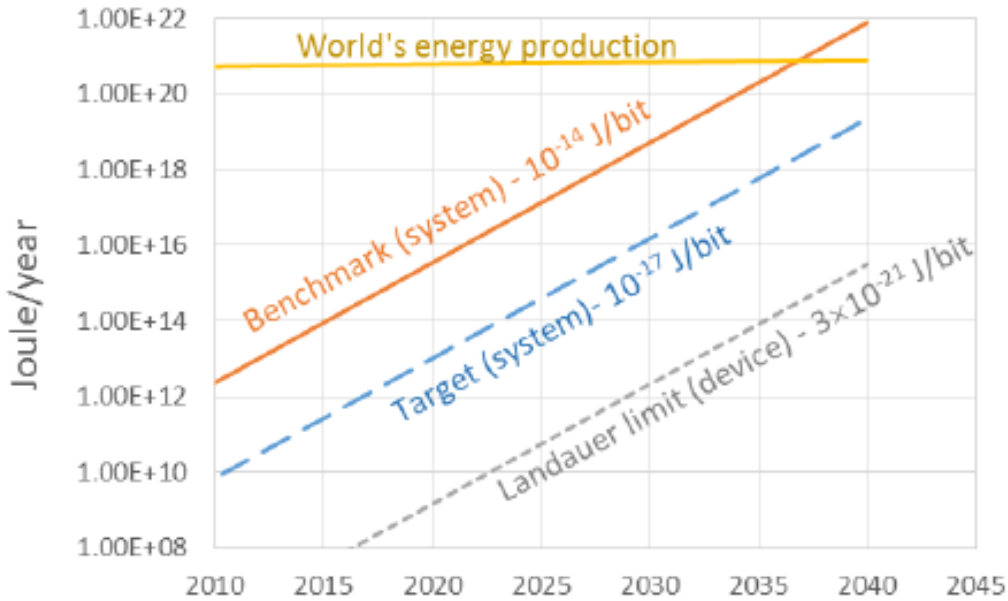
Figure 1: Total Energy of Computing (SIA, 2015)

While the above techniques at minimizing the energy consumption in digital devices goes some way toward curbing the rapidly growing energy drain on society that the digital age is forcing us to confront, these techniques will not work when designing future artificially intelligent computational architectures inspired by human brain function. For starters, while miniaturization has worked well in the digital realm, the size of neurons in the mammalian neocortex have remained relatively unchanged for the past 200 million years. While that is not to say that computing architectures designed around the structure of the brain will not benefit from miniaturization, it is notable that this is *not* how the brain developed such massive computational and energy efficiency. Similarly, the brain does not manage its energy consumption through tricks such as power gating or varying its voltage parameters. The reason for this is that, as a massively parallel architecture, it is not possible to cut power to any part of the brain without seriously disrupting the function of the entire organ. In addition, and as we will see later, efficient brain operation depends greatly on managing similar voltage fluctuations across its elements (neurons) in order to produce coherent brain rhythms. Therefore, a "dual voltage" option would not be a useful feature to incorporate into an artificial brain.

In short, while the brain is undeniably a highly computational and energy efficient machine, it manages to accomplish this feat through some mechanism(s) unfamiliar to contemporary electrical and computer engineering practices. As such, it would seem that an investigation into the mechanism the brain does use to manage its computational and energy efficiency would be of interest to the future generation of engineers looking to the biological wisdom of the human brain for guidance. Indeed, in a recent article in the popular electrical-engineering trade journal, *IEEE spectrum*, no fewer than three articles pointed out that, even though the human brain has a computational capacity far outweighing even the largest of today's supercomputers, it operates at a tiny fraction of the energy consumption of these big computers (Hasler, 2017; Meier, 2017; Rothganger, 2017). Therefore, if we are to address the rapidly growing energy drain on society that the proliferation of computing devices is bringing upon us, it is essential that researchers and

engineers soon put forth a serious effort to understand just how it is that human brain efficienty manages its computational and energy efficiency.

Indeed, this is exactly what our team is doing at the Biologically Inspired Neural and Dynamical Systems (BINDS) lab at the University of Massachusetts, Amherst. In our group within the lab, the "Neuro-energetics" group, we have developed a mathematical model/computer simulation of what we are arguing is the basic metabolic/computational functional unit within the human cerebral cortex. This unit, what we call the "Capillary-Astrocyte-Neuron (CAN)" unit is roughly equivalent in size and structure to the canonical "cortical column" identified by Mountecastle (1997) as the primary granular or atomistic functional module/unit of cortical operation. In the CAN unit model and its accompanying Matlab computer simulation, we attempt to replicate the complicated cycle of energy flow through the unit by simulating the fluxes of energy precursors and metabolites between the elements of the unit, the electrochemical gradients established across the unit's constituent neuron, and the integrate-and-fire properties of the neuron in its association with other neurons in the assemblage.

In light of these limitations of existing models, we have developed the Capillary-Astrocyte-Neuron (CAN) unit model, which addresses the three above-raised concerns. In addressing the first concern, what we have done is to "reduce" the several-dozen equations and parameters of the models described above relating to the metabolic portion of the feedback loop into two differential equations with four parameters. We then compartmentalize these two equations along with the vasculature into one compartment of a two-compartment model. For the second compartment, we adopt the framework of Izechivich's (2003, 2007) "simple-spiking neuron model" which, in the spirit similar to our reduction of the metabolic equations into two differential equations, reduces the more complicated Hodgkin and Huxley related equation sets into two simple differential equations. The end result is that we have constructed a model of a patch of cortical neuropil which simulates the complex feedback flow of metabolic energy through that patch along with a description of how that feedback flow affects the spiking behavior of the individual neuron in relation to the input influences impinging on it from other units in the local pool. Extending the model even further, we have constructed an 8x8 array, *in silico*, of 64 of these CAN units to simulate the mesoscopic dynamics of a small region of neocortical tissue representative of a mammalian-brain primary sensory receiving region such as the primary visual cortex (V1) or olfactory bulb.

Put simply, the CAN-unit model is a two-compartment model with a metabolic component combining the cerebral blood flow (CBF) contribution with the astrocytic glycogen store and mitochondrial production of ATP, and a second component being the spiking neuron component. Each individual "CAN" is modeled by one capillary, one glia cell (astrocyte), and one neuron. While a somewhat simplified characterization, there is evidence that suggests that there is a one-to-one relation between the number of capillaries in the brain and the number of neurons there (van Tellingen et al. 2015), each being on the order of 100 billion. While an individual CAN involves a single capillary-astrocyte-neuron as described above, a "CAN-unit," as we call it, corresponds roughly to a functional unit or "module" of cortical function referred to as a *cortical column* (Mountcastle, 1957, 1978, 1997). While there is ample evidence that the mammalian cortex is "granularized" in the form of interacting cortical columns, there continues to be a debate as to the scope of functionality of these units and especially how to define them

cytoarchitectonically (Haueis, 2016; Rockland & Ichinohe, 2004; Rockland, 2010; Ts'o et al., 2009). Even so, it is important to state for this paper explicitly what constitutes a functional cortical column in the effort to describe how they interact in a larger hierarchical framework. For example, the canonical *cortical column* that Mouncastle (1957) discussed back in 1957 has been scaled up and down and redefined a number of times over the decades to the point that the standardization of terms is suspect. That is, in addition to authors using the term cortical "column" to stand for a functional unit of cortical function, they also use microcolumn, minicolumn, macrocolumn, and hypercolumn. Again, there is no widespread agreement on how to define each of these terms cytoarchitectonically (Rockland and Ichinohe, 2004; Tso et al. 2009). That said, a good way to bifurcate the scale of the cortical column is to divide it into minicolumns and macrocolumns. The minicolumn contains roughly 100 neurons and has a diameter of roughly 50 μm. The macrocolumn is composed of roughly 100 minicolumns, contains about 10,000 neurons, and has a diameter of roughly 4-500 μm (Rockland, 2010). In each case, the principal concept of the cortical column is that is represents a "receptive field" of the detection of some sensory stimulus in an animal's environment (see section 4.2). For the purposes of this paper, we are defining a CAN unit as having 1000 neurons. We defined the CAN unit in this way not only because it is a mediary between a mini and a macrocolumn, but principally because the existing Izhikevich simple spiking model that we have incorporated into our model uses a 1000 neuron pool simulation. In future simulation work, we may adjust the definition of the CAN-unit as necessary for optimization of information-processing purposes.

The tentative conclusion we have to after working with the model and its simulation is that the method by which the human brain is able to perform such sophisticated computational feats at such a low energy cost is through 1) coordination of delivery of energy molecule precursors to cooperatively interacting cortical regions, and 2) the phase synchrony in the oscillations of dendritic currents in the CAN unit neuron collectives that populate these interacting cortical regions. More specifically, we argue that the coordinated delivery of nutrients to cooperatively interacting cortical regions set a tempo of the restoral of the resting membrane potential in their constituent neurons which help facilitate the cooperative phase-synchronized, narrow-band oscillations seen between these cooperatively interacting regions. In order to breakdown the CAN unit model into digestible bites, we will first discuss the justification for the model. Specifically, we will discuss the justification for simplifying the very complicated process of biological-cellular and neurophysiological cortical column dynamics into a few simple equations. Then, we will introduce the "power-grid" metaphor of CAN unit dynamics in order to help facilitate a more user-friendly visualization of the dynamics of the model. After that, we will outline the mathematical equations used in the CAN model as well as some simulation results. Finally, we will discuss what our goals are for future research in the area of neuroenergetics and brain dynamics.

2. Neuroscience Background

Over the past two decades, remarkable advances have been made in non-invasive methods to study mammalian brain function--human brain function in particular (Bandettini, 2009; Moseley et al. 2009; Soares et al. 2016; Tewarie et al. 2016). With these new non-invasive techniques have correspondingly come new demands on the methods in which researchers are finding themselves having to model those brain processes. For example, neuroscience research in the

twentieth century could be referred to as the age of "neuron-centered" investigation as to the manner in which brain tissue processes information there (Kozma & Freeman, 2016; Millet & Gillette, 2012; Guillery, 2005). Early techniques for studying brain function focused mainly on "stimulation-ablation" experiments whereby selected portions of an animal brain were destroyed or electrically stimulated in a generally crude and naïve fashion, and the behavior of the animal observed and described. Later on in the century, more sophisticated techniques were developed to stimulate and record individual neurons and small populations of neurons *in vivo* through surgically implanted electrodes in an animal's brain (Haueis, 2016). In human's, however, the only access to brain activity was essentially from the relatively crude EEG recordings produced by scalp electrodes, with the partial exception of a small sample of intracranial electrocorticogram (ECoG) studies conducted on patients undergoing surgery for intractable epilepsy (Freeman et al., 2000; Holmes et al,. 1996; Ojemann et al., 1988; Ojemann et al, 1992).

While the majority of brain studies in nonhuman animals continue to be of the invasive variety described above (e.g., Insel & Barnes, 2015; Schneider & Woolley, 2010), the twenty first century has seen a dramatic change in the manner in which human brain processes are being studied. This change is a direct result of new non-invasive neuroimaging techniques such as fMRI, MEG, DTI, PET and others (Bandettini, 2009; Shibasaki, 2008). A fundamental difference between the data obtained from fMRI studies and those obtained from traditional invasive recording techniques is that the former looks at the blood-flow fluctuation patterns in brain activity while the latter essentially records spiking behavior from neurons alone. Considering such, researchers have spent the majority of the past two decades trying to justify a link between these hemodynamic fluctuations, dubbed the Blood-Oxygenated Level Dependent (BOLD) response, and the individual-spiking and population-dynamics behavior of associated neurons. Indeed, over that two-decade period a positive relationship has been found between neural activity in a given brain region and the corresponding BOLD fluctuations in that region (Bandettini , 2012; Norris, 2006; Van den Heuvel & Hulshoff, 2010). What has also been found in that two decade period, however, is that the perceptual and cognitive information-processing operations of the brain are not so simply described *solely* by the interaction of discrete neuron elements, but rather are better described by a much richer interaction between those neurons and the supporting glia cells and vasculature that composes the cortical neuropil (Moore and Cao; Chevy; Zonta).

Accordingly, there has been recent interest in modeling complicated interactions and feedback pathways between these elements of cortical neuropil (Aubert & Costalat, 2002; Aubert & Costalat, 2005; Bélanger et al., 2011; Filosa et al., 2004; Kannurpatti, 2017; Mangia et al., 2009 Mason, 2017; Mesquita et al., 2009; Sickmann et al., 2009). Drawing on these and other recent empirical studies in the literature, several groups have begun to develop detailed mathematical models of the relationship between cerebral blood flow, astrocytic, and neuron metabolic interactions (Chander & Chakravarthy, 2012; Cloutier et al., 2009; Jolivet et al. 2015; Mangia et al. 2009). While each of these efforts represent a heroic first attempt at modeling the relationship between metabolic activity in the cortex and neuronal function, extending these models to reflect the information-process capacities of the brain will prove troublesome for three reasons: One, biologically realistic-seeking mathematical models are often overly complex and include too many equations and parameters to comfortably simulate the tens to hundreds of thousands of interacting functioning units that comprise even a small region of cortex (Chhabria &

Chakravarthy, 2016; Izhikevich, 2003; Noack et al. 2017). That is, each of the models described above are composed of several dozens of equations and many more parameters. Two, with the exception of (Chander & Chakravarthy, 2012), while describing how neural activity affects the glia cells and vascular system in a "forward" direction (following Chander & Chakravarthy, 2016a) by affecting glucose consumption and capillary dilation, the above models are short in describing how the "reverse" aspects of energy supply to the neuron from the glia and capillaries affect the ongoing spiking behavior of the neurons in relation to inputs from other neurons in a network. Three, the above simulations only model the biology of a single metabolic-neuronal unit in isolation. The coordination of many such units forming a population are likely to affect the behavior of any individual target unit with the effect that the parameters defining the simulated-isolated individual unit would likely be different from that unit participating dynamically in a population. These crucial influences are not considered in the parameterization of the models.

3. Proposed metabolic-neural model: CAN

3.1 Previous work related to the CAN model

As discussed earlier, while there has been a recent surge in the number of reports describing how neural activity in the mammalian forebrain affects the cerebral blood flow BOLD response, there have been many fewer studies reporting on the reverse effect as to how the energy supply neurons receive through the vasculature and astrocyte glycogen pools affect their ongoing spiking behavior. In fact, it is arguable that there has only been one comprehensive effort in this direction, carried out by the team of Chhabria & Chakravarthy (2016; see also Chander & Chakravarthy 2012; Philips et al. 2016). There are several similarities between Chhabria and Chakravarthy formulation, which we can call the neuro-glio-vascular (NGV) model. One, they have recognized that, in order to comfortably simulate the large number of "units" that will be necessary to model human-cortical information processing is necessary to reduce or "low dimensionalize" the 89 or so equations they formulated for the metabolic portion of the model Chhabria & Chakravarthy (2016). Effectively, they have condensed their low-dimensional simulation into a two-component model, where one component is a "lumped" glio-vascular system and the second compartment is the spiking-neuron system. We have constructed essentially the same general framework. The second general similarity between our two models is that we see the effect of ATP production as the principal factor connecting the two (glio-vascular and neuron) systems.

Where the models differ, though, is in the larger interpretation of exactly how ATP regulates not only the spiking behavior of the single neuron but, even more importantly, the population behavior within and especially between CAN units. In the NGV model, the influence of ATP in the neuron is effectively to set a neuron firing "threshold;" as Chhabria and Chakravarthy (2016) state:

> "The main intuitive idea behind the … model is that ATP controls the firing threshold of the neuron. The threshold is low for high ATP levels and increases under low ATP or energy-starved conditions."

This concept is similar to one that recently came out of BINDS lab (Burroni et al., 2017). The main idea in that research effort was that there is a pool of energy available to the spiking

neurons in the network. That energy comes in the form of ATP and in compromised dietary conditions such as hypoglycemia, the threshold level for a given neuron firing is similarly raised as in the NGV model. While this is a sound, intuitive idea, we envision a somewhat more complex role for ATP in that we see the entire energy cycle as manifesting a "rhythm" in which the availability of ATP coordinates the spiking behavior of neurons in local units through modulating the timing of the restoral of the neurons resting membrane potential.

Another important way in which the CAN-unit models differ from the NGV model is in the characterization of the spiking neuron portion of the simulation. We have chosen to use Izechevich's simple spiking neuron model whereas (Chhabria and Chakravarthy, 2016) has chosen to use a quadratic integrate and fire model. Finally, our models differ in their approach to characterizing the larger cortex-wide information-processing philosophy. Chhabria and Chakravarthy (2016) adopt a relatively standard generative neural network formulation modeled as an "auto-encoder" (Philips et al., 2016). The CAN-unit model, on the other hand, relates to Katchalsky set model (Kozma, Freeman, 2016), which is derived from over a half-century of pioneering experimental neurophysiological work by Walter Freeman (1975), and which is more biologically plausible than the back-propagation related approach (Philips et al., 2016).

3.2 Metabolic component of the CAN model

The metabolic portion of the model is inspired by (Coutier et al., 2009; Jolivet et al., 2015) and others, the principal challenge was in deciding which of the biological processes described by the multitude of equations and parameters to include in the CAN model. We decided that the important features of the (Cloutier et al., 2009) model we wanted to preserve were 1) the flux of glucose from the CBF to astrocyte, 2) the capacity through which the astrocyte can store this glucose energy reserve in form of glycogen (while the neuron cannot), 3) the "astrocyte-neuron lactate shuttle," the mechanism whereby the astrocyte breaks down its glycogen stores to deliver energy in the form of lactate to the neuron in times of need, and 4) the process whereby the neuron metabolizes lactate in the mitochondria to produce ATP, which, in turn, powers the neuron's sodium-potassium pumps.

In short, we were able to reduce the 50 or so equations in the (Cloutier et al., 2009) model into two differential equations. The first equation describes the rate of change of the state variable, g, which is a measure of glycogen/energy store in the astrocyte available for the neuron to utilize. The second equation describes the rate of change of the state variable, m, which is a measure of the ATP available to reset the membrane potential of CAN unit's representative neuron. From here, we coupled our above formulation, the "reduced Cloutier model," to the canonical IZ model through a parameter in the IZ model related to the resetting of the membrane potential and the m state variable of the reduced Cloutier model.

The mathematical portion of the CAN unit model is composed of four coupled differential equations. The first two are a "reduced" representation of the roughly 50 differential equations which comprise the Cloutier et al. metabolic model, while the second two are essentially identical to the canonical IZ model, with the exception of the added "βm" term in equation (4) that serves as the main state variable that couples the IZ model to the reduced Cloutier at al. model. As for the metabolic part, we have the following equations:

$$\frac{dg}{dt} = \varepsilon v \frac{S}{\tau_m} - \frac{\gamma g}{1+m} \qquad (1)$$

$$\frac{dm}{dt} = \frac{\gamma g}{1+m} - \mu m \qquad (2)$$

Equation (1) represents the glycogen stores in the astrocyte portion of the CAN unit immediately available to the neuron as energy to drive the neurons' Krebs cycle in the production of ATP there. $D(g)/dt$ reflects the change in the glycogen concentration in the astrocyte as a function of the glucose delivered there via the cerebral blood flow (CBF), represented by the expression $\varepsilon v(S/\tau_m)$, as well as the ratio of available glycogen stores (g) in the astrocyte to the current concentration of ATP in the neuron. ε and γ are proportionality constants, and S is a reflection of the level of synaptic activity on the neuron dendrites of the neuron portion of the CAN unit. As the CAN model in its current form is a fully connected network, S represents the summation of the membrane potential values (thresholded by 45mV) of the neuron, V, from whenever it spikes across 100 times steps. This average is divided by τ_m (100ms), to give an average value of the potential over a 100 ms epoch. The significance of the value of S lies in that it is used here to represent the concentration of the excitatory neurotransmitter glutamate in the synaptic clefts and interstitial matrix of the CAN unit, which has been shown to influence the constriction and dilation of the capillary portion-CBF flow of the CAN unit (Bélanger et al. 2011). The last term in the equation, ($\gamma g/1+m$), reflects the ratio of available glycogen stores, (g), in the astrocyte to the current concentration of ATP in the neuron. Higher values of (g) will attenuate the rate of increase of glycogen stores relative to the contribution by the CBF. Higher values of (m) indicate that the neuron is currently flush with ATP and so acts to increase the buildup of glycogen stores (g).

Equation (2) represents the ATP availability in the neuron to be used in the restoration or resetting of the membrane potential there. The restoration of the membrane potential consumes the majority of the ATP in the neuron cell and is responsible for the efficiency whereby the neuron performs it's critical "integrate and fire" duties. The state variable in this equation is (m), and the term $d(m)/dt$ reflects the change in the concentration of ATP in the neuron available to reset the membrane potential through driving the neuron's sodium-potassium pump. As in equation (1), the term ($\gamma g/1+m$), reflects the ratio of available glycogen stores in the astrocyte to the current concentration of ATP in the neuron and serves a similar regulatory role as in equation (1). In relation to this equation (2), higher values of m indicate a relative saturation of ATP in the neuron and, thus, will attenuate the rate of increase in ATP production. Higher values of g indicate that, should the concentration of ATP (m) in the neuron be low, there is a large supply of glycogen (energy) that the neuron can utilize to produce more ATP. Thus, larger ratio of g/m in this equation will drive a positive rate of change of ATP production. The ($-\mu*m$) term reflects the exponential decay of m as parameterized by the constant μ. The exponential decay is modeled as a process whereby ATP is continually consumed by the neuron as a steady function

of the demand of the sodium potassium pumps to reset the resting membrane potential. Having this term present in the equation is also essential for the simulation to produce oscillatory behavior in the metabolic network.

3.3 Description of the parameters, variables from Izhikevich and Metabolic modules
This contains all the variables and parameters from equations 1, 2, 3, 4 as well their descriptions and value/range of values.

Table I.
Parameters and Variables of the CAN Model

Variable/ Parameter	Description	Value/Range
ε	Coupling parameter from spiking neurons to glucose concentration in blood stream.	[0, 0.1]
S	Sum of the membrane potential of a neuron (with threshold of 45mV) from all the times it spikes in last 100 milliseconds.	[0, 4500] mV
τ_m	Time span of metabolic cycle	100 ms
ν	Coefficient related to blood flow	0.5
γ	Coefficient related to glycogen balance	0.3
μ	Coefficient related to ATP balance	0.3
β	Energy-to-spiking coupling factor	[0, 0.5]
σ	Connectivity strength between neurons in the Izhikevich model	Value from uniform random distribution between 0 and 1 for connection strengths from excitatory neurons and value from uniform random distribution between 0 and -1 for connection strengths from inhibitory neurons.
v	Cellular membrane potential in the Izhikevich model	[-65, 45] mV
u	Membrane recovery variable in the Izhikevich model	[116, 30] mV
I	Input current to each cell in the Izhikevich model	Random value from standard normal distribution (std 0.5 or 0.2)
b	Sensitivity of the recovery variable u to the sub threshold fluctuations of the membrane potential v in the Izhikevich model	0.2 for excitatory neurons and 0.25-0.05 uniformly distributed random value for inhibitory neurons

3.3 Spiking NN component of the CAN model

The typical first step in any effort to model a biological process is to review the available preceding literature/studies on the subject. What we found was that, while there was a good deal of research, *separately*, on the cellular biology of neurons/glia removed from spiking behavior, and research focused on spiking behavior solely, there was essentially no research done on integrating both. Therefore, in initializing this project, we were forced to try to create some sort of manageable hybrid of both the metabolic approach to neurobiology and the more information-processing approach exemplified by the canonical single-neuron "leaky integrate and fire (LIF)" or spiking neuron models that typically eschew any discussion of energy constraints on spiking behavior. The end result of our deliberations on what strategy to use to attack this project was to try to reduce the 50 or so differential equations used to describe the neurobiology of the brain-astrocyte-neuron assemblages in the neocortex reviewed in the Cloutier et al. (2009) model and merge it with the already simplified Izhikevich (IZ) model (2003) of simple spiking behavior in cortical neurons.

More specifically, we drew inspiration from IZ's approach to reduce the prohibitive number of equations and parameters in the biologically motivated Hodgkin and Huxley model and related models to simulate the spiking behavior of individual neurons and small populations of interacting neurons.
 In his landmark 2003 paper, IZ published a simplified spiking model of this simple neuron spiking behavior as well as the code to run a simulation of 1000 fully connected neurons. What was especially notable about this effort was that, unlike more simplified LIF neuron models, the reduced IZ formulation boasted the capacity of this simplified model to not only simulate what he referred to as the "regular spiking (RS)" behavior of the typical neocortical neuron, but also the behavior of a collection of other, specialized neurons found in various regions of the telencephalon, such chattering neurons, intrinsically bursting neurons, low-threshold spiking neurons, and others (IZ). The IZ equations are given as follows:

$$\frac{dv}{dt} = 0.04v^2 - 5v + 140 - u + I(t) \tag{3}$$

$$\frac{du}{dt} = -0.02u + 0.02v(b + \beta m) \tag{4}$$

Equation 3 is one half of the canonical IZ simple-spiking neuron model and has been unchanged in the current formulation of the CAN model. The state variable in this equation is V, and dV/dt reflects the rate of the change of the membrane potential across the CAN unit neuron as a function of the values of the variables U and I(t). The first portion of the equation combine three terms into the expression $(0.02V^2 + 5V + 140)$ which has been carefully formulated by Izhikevich (2003) to produce biologically realistic firing patterns in individual neurons and small population of neurons. The parameters which affect the specifics of the spiking behavior are found in the two terms that follow it, u and I(t). I(t) represents the influences of the other neurons' axons in the network impinging on the CAN unit target neuron in question. The influence of I(t) can be divided into positive and negative effects depending on whether the input

is coming from the excitatory neurons or inhibitory neurons of the network Greater values of I(t) will drive dV/dt higher as it reflects a greater contribution of excitatory synaptic activity. The term U is the state variable of equation (4) and its function is to modulate the value of V by counteracting the depolarizing effect of high I(t) values. It (U) represents the actions of ATP on the neuron's sodium-potassium pump in the effort to restore the resting membrane potential to a value of -70 mV. Parameter b represents the sensitivity of the recovery variable u to subthreshold fluctuations.

Equation 4 is the second half of the canonical IZ simple-spiking neuron model and has been slightly modified in order to couple the IZ spiking-neuron model to the Cloutier portion of the model. What has been added is the (β*m(t)) term, which reflects the contribution of the time-varying concentration of ATP stores in the spiking dynamics of the canonical IZ model and simulation. The state variable in this equation is U, and d(U)/dt reflects the strength through which the neuron's resting membrane potential is reset or more specifically, is *resistive* to the depolarizing effects of high excitatory neuron I(t) values in equation (3). Again, the first two terms in the expression (-0.02U + 0.02V(b)) are taken unchanged from the canonical IZ model. The last term, (0.02*V*(β)*m(t)) relates the scaling factor (β) to the current concentration of ATP in the neuron available to do work running the neuron's sodium-potassium pump in the effort to restore the neuron's resting membrane potential.

3.4 Coupling the metabolic and spiking neural components

While this early form of the CAN model, what we originally called the "reduced IZ-Cloutier" model, showed some interesting behavior in single neuron simulations with a steady metabolic input, it only modeled an open-form flow of energy from the vascular system, through to the astrocyte and neuron, ultimately culminating in its influence on the spiking behavior in the IZ network through the metabolic portion affecting the spiking behavior and frequency of the neuron through its effect on resetting the neuron's membrane potential. In order to close the form of the system of equations, we added a term in the first equation modeling the g variable, which represented the glutamate concentration in the interstitial matrix surrounding the CAN unit's representative neuron. In experimental studies (Bélanger et al. 2011), this concentration, which is reflective of the metabolic activity of the CAN unit neuron, is sensed by the CAN unit astrocyte and serves to compel that astrocyte to dilate the capillary portion of the CAN unit. Dilating the capillary then serves to deliver more glucose to the astrocyte in response to the increased need for energy precursor molecules demanded via the increased activity in the CAN unit.
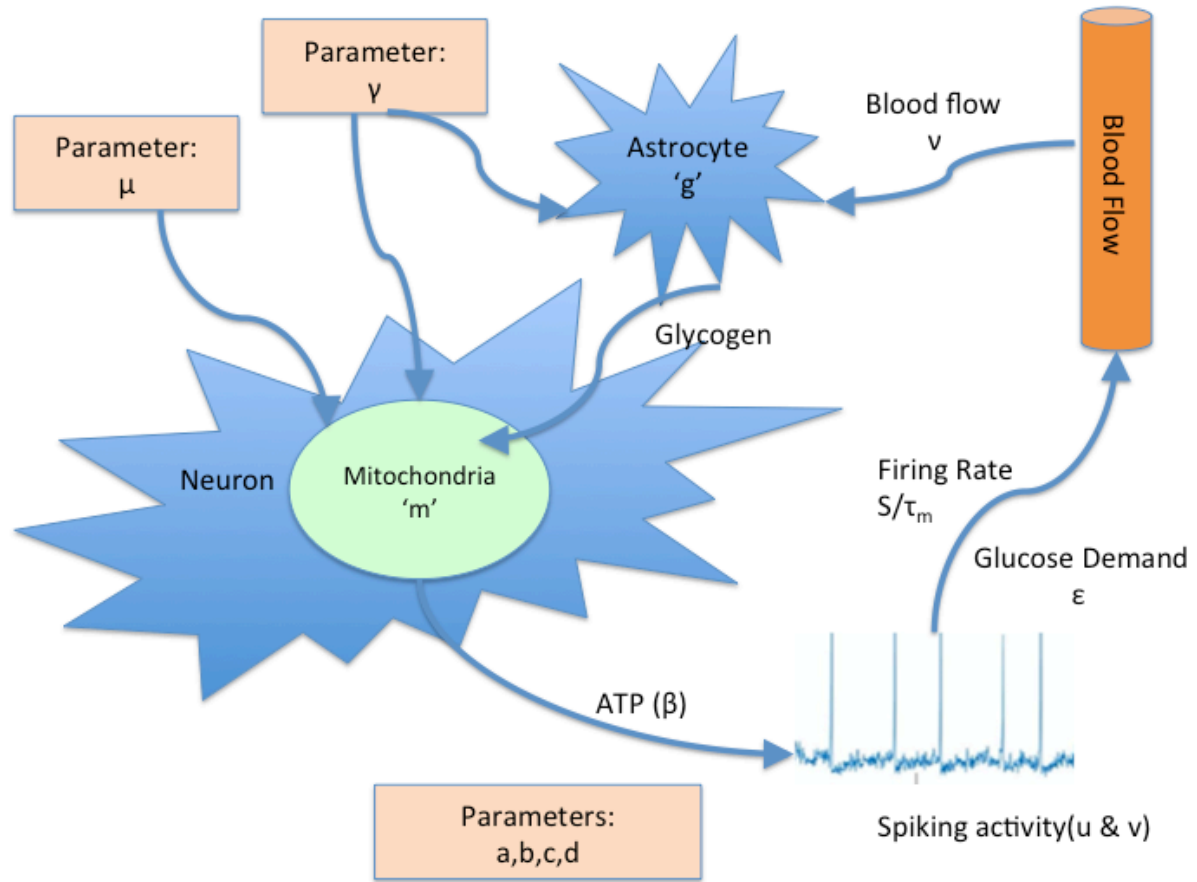
Figure 2: Schematic representation of the CAN unit model showing the flux relations between its various components.

4. Computer simulations of CAN models

4.1 Single CAN units

Simulation runs of the CAN-unit model were carried out using MATLAB. Our efforts in this paper focused on finding optimal parameters which produced robust gamma oscillatory behavior in each CAN unit while keeping the values of the energy related (m) and (g) state variables "well behaved" and normalized between the values of 0 and 1. The reasons we chose these criteria to govern the parameterization of the model is 1) robust gamma oscillations are a defining characteristic of *in vivo* ECoG or local field potential recording in brain cortical columns, and 2) "non-well-behaved" values of (m) and (g) that stray outside of the normalized range often shift the behavior of the IZ spiking neurons into that of a "chattering mode," which is more characteristic of non-cortical neurons rather than the "regular spiking" behavior of cortical-pyramidal neurons.

4.1.2 Regions of Interest

A constraint imposed on the model is that the variables 'm', 'g' for all neurons needed to be within the range [0,1]. Hence, the goal was to find values of β, ε in the parameter space that satisfied this criterion. An exhaustive search of the parameter space was done for β in the range [0,0.5] and ε in the range [0, 0.7]. The regions in the parameter space that satisfied the restriction for values of 'm', 'g' could be roughly divided into two regions of interest (ROI) we describe as RO1-1 and ROI-2. ROI-1 consists of points in the region β = [0, 0.5], ε = [0, 0.1]. Plots detailing the properties of ROI-1 are shown and described below. ROI-1 has points for which we can sufficiently modulate the power in the gamma band, have high synchrony while satisfying the constraint for values of 'm', 'g'. ROI-2 consists of points in the region β = [0, 0.1], ε = [0, 0.5]. However, this region does not have areas with high synchrony with the ability to modulate power in the gamma band that satisfy the constraint for the values of 'm', 'g'.
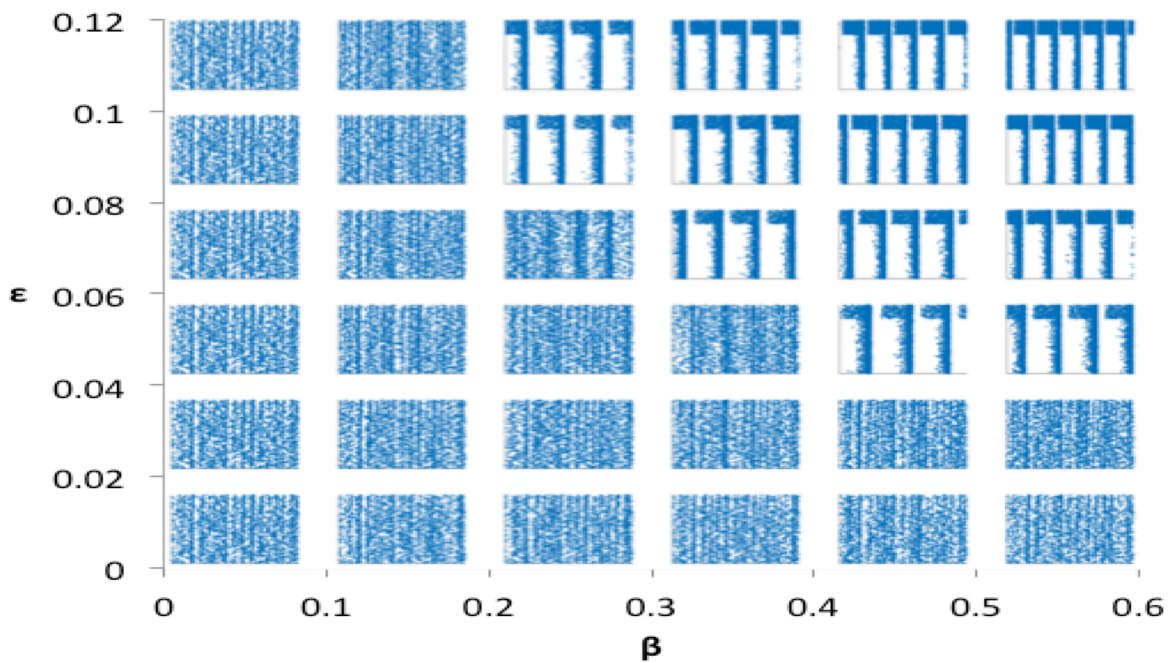

Figure 3: The plots in this figure correspond to different values of β and ε in ROI-1 that are sampled at intervals of 0.1 for β and intervals of 0.02 for ε and arranged in increasing values of β and ε. The x-axis represents the index of the neuron and the y-axis represents the time step which ranges from 0 to 500 ms. The plots in the upper right corner are hyper synchronized and due to this there is a clear 'beating' pattern, which can be observed. There is a sudden transition from relatively low synchrony to high synchrony and we can observe a sharp boundary between low and high synchrony.
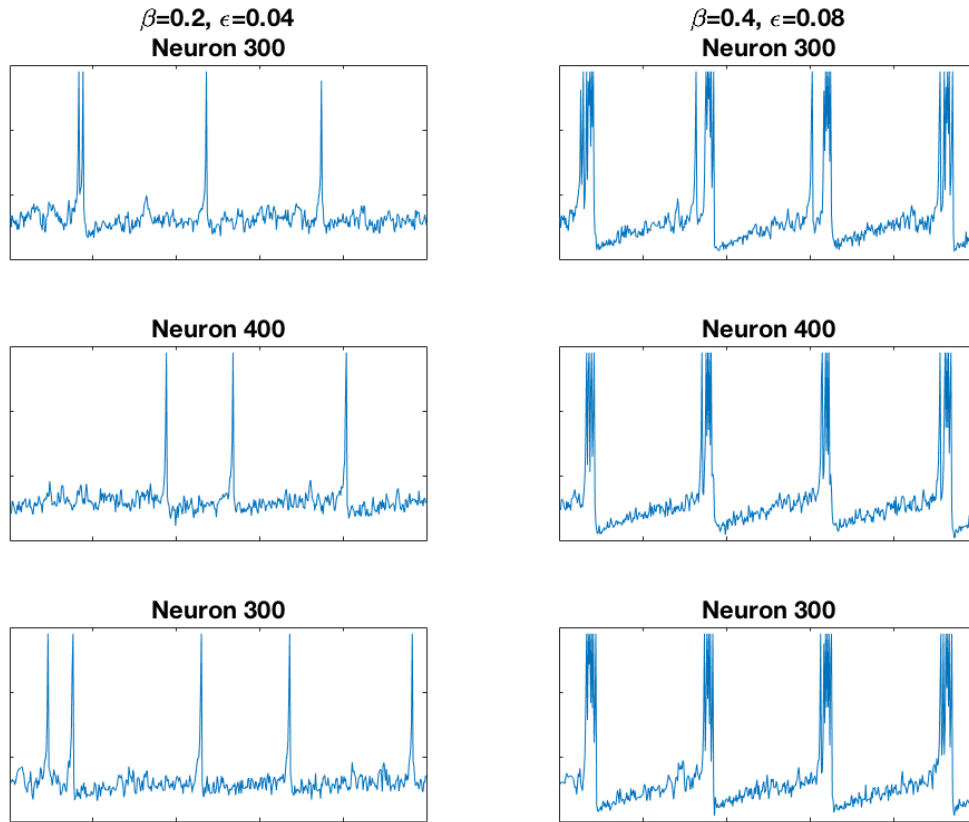
Figure 4: The plots in this figure can be divided into two columns based on the values of β, ε. Each plot represents the spike train of a specific neuron for a timespan from 1 to 500 ms. The first column corresponds to β = 0.2, ε = 0.04 and the second column corresponds to β=0.4, ε=0.08. The first row represents 500th neuron, the second row represents the 400th neuron and the third row represents the 300th neuron. The behavior seen in the first column can be described as tonic spiking. The behavior seen in the second column can be described as chattering. In the second column it can be observed that the spikes are much more synchronized between the different neurons compared to the first column, as the individual spikes are more in line with one another.
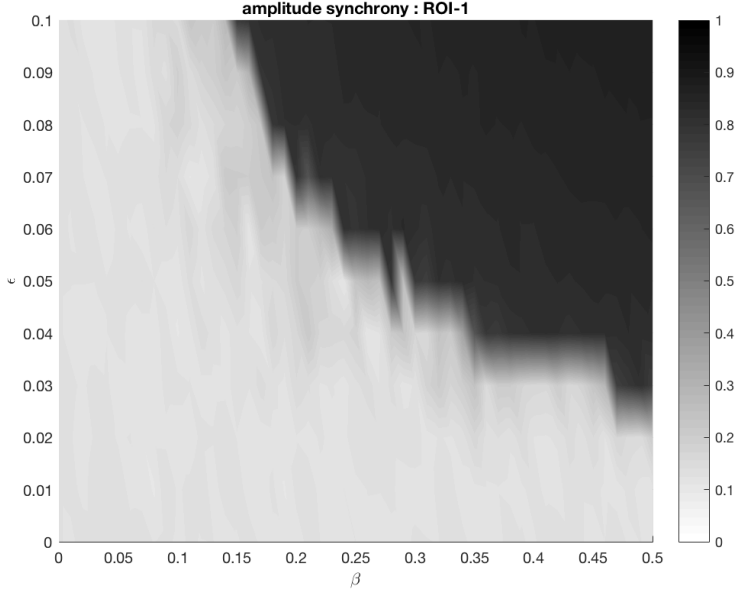
Figure 5: Synchrony over ROI-1. The darker regions represent higher synchrony among the firing activity of the different neurons and the lighter regions represent lower synchrony among the firing activity of the neurons.

The metric plotted against (β, ε) in Figure 5, denoted as $\chi(N_e)$, represents the amplitude synchrony among the N_e excitatory neurons. It is derived as follows:

V(t), the global mean membrane potential at time 't' for the N_e neurons is obatined by finding the mean membrane potential at every time-step.

$$V(t) = \frac{1}{N_e} \sum_{i=1}^{N_e} v_i(t)$$

The variance, σ_V^2, of the global average membrane potential across timespan, T, from 1 to 1000 milliseconds is derived as:

$$\sigma_V^2 = \frac{1}{T} \sum_{t=1}^{T} V(t)^2 - \left[\frac{1}{T} \sum_{t=1}^{T} V(t) \right]^2$$

The variance, $\sigma_{v_i}^2$, of the membrane potential of the ith neuron across timespan T, from 1 to 1000 milliseconds is derived as:

$$\sigma_{v_i}^2 = \frac{1}{T} \sum_{t=1}^{T} v_i(t)^2 - \left[\frac{1}{T} \sum_{t=1}^{T} v_i(t) \right]^2$$

The amplitude synchrony among the excitatory neurons, $\chi(N_e)$, is obtained using σ_V^2 and $\sigma_{v_i}^2$ as follows:

15

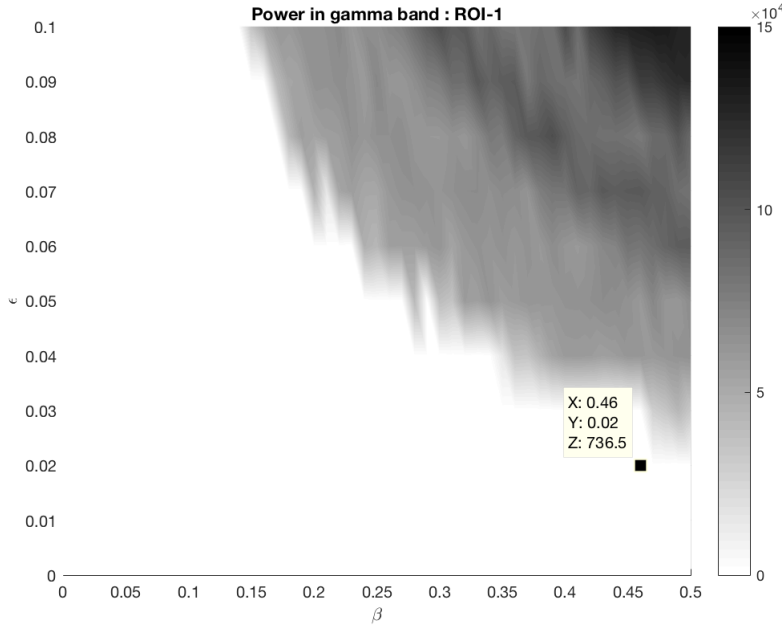$$\chi(N_e) = \sqrt{\frac{\sigma_V^2}{\frac{1}{N} \sum_{i=1}^{N} \sigma_{v_i}^2}}$$

Figure 6: Gamma modulation ROI-1. The above figure is a surface plot in which power in the gamma band, $P_{\mu_{gamma}}$, is plotted against β,ε. The darker regions represent higher power in the gamma band and the lighter regions represent lesser power in the gamma band.

The metric against (β, ε) in Figure 6, denoted as $P_{\mu_{gamma}}$, is derived as follows:

We obtain the mean membrane potential, v_{i_μ}, for i^{th} excitatory neuron across timespan, T, from 1 to 1000 milliseconds using the time series of the membrane potential signal, $v_i(t)$.

$$v_{i_\mu} = \frac{1}{T} \sum_{t=1}^{T} v_i(t)$$

The mean subtracted time series, $v_{i-\mu}(t)$, of the membrane potential of the ith excitatory neuron is obtained by subtracting the mean membrane potential, v_{i_μ}, from the membrane potential signal, $v_i(t)$, at each time step.

$$v_{i-\mu}(t) = v_i(t) - v_{i_\mu}$$

The mean time series, $v_\mu(t)$, of the mean subtracted membrane potential signal, $v_{i-\mu}(t)$, across all, N_e, excitatory neurons is obtained as follows:

$$v_{\mu}(t) = \frac{1}{N_e} \sum_{i=1}^{N_e} v_{i-\mu}(t)$$

$v_{\mu}(t)$ is filtered by a band-pass gamma filter with passband from 40Hz-60Hz to obtain the filtered mean signal with just the gamma component $v_{\mu_{gamma}}(t)$.

The power in the gamma band, $P_{\mu_{gamma}}$, is computed as sum of the squared value of the gamma-filtered signal, $v_{\mu_{gamma}}(t)$, across timespan, T, from 1 to 1000 milliseconds.

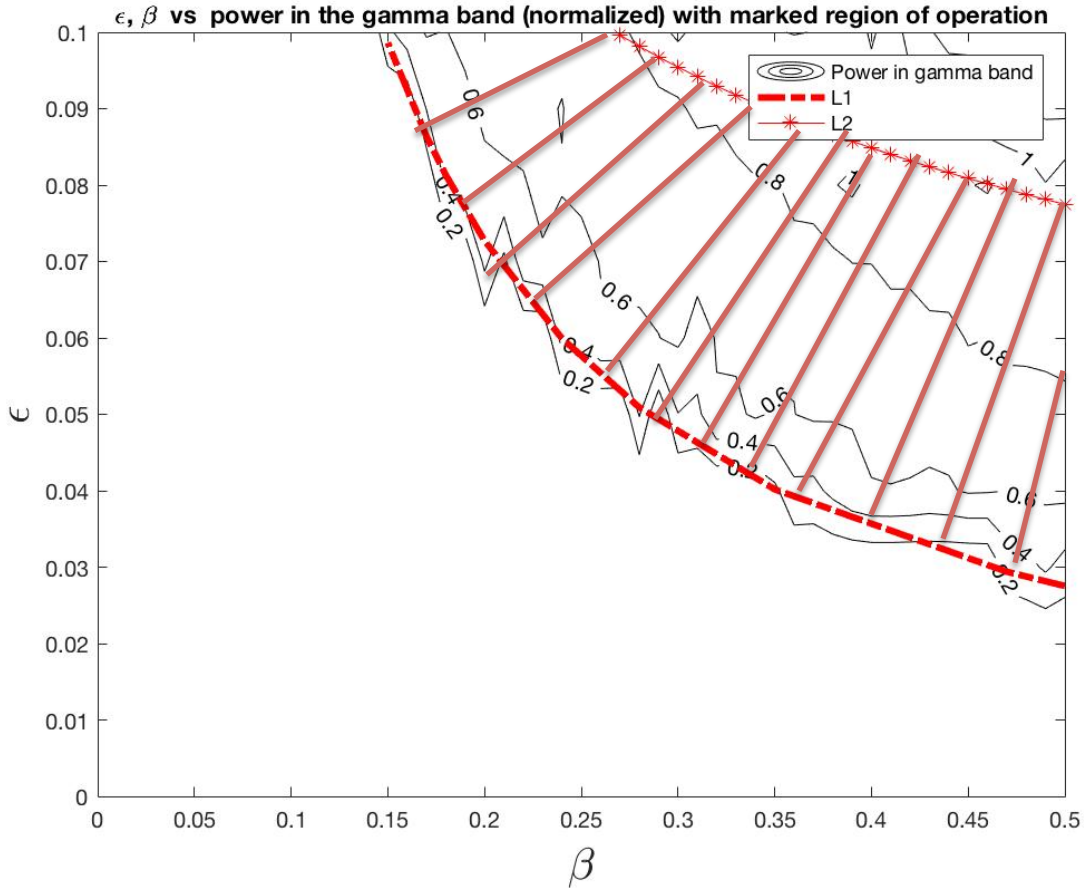$$P_{\mu_{gamma}} = \sum_{t=1}^{T} v^2_{\mu_{gamma}}(t)$$

Figure 7: Contour plot for ROI I (showing limits with fitted red lines)

The shaded region in Fig. 7 between L1 and L2 represents the region of operation in ROI-1. It consists of all those points in the parameter space of β, ε where for which there is high synchrony among the neurons in the column and where we can modulate the amount of power in the gamma band with 0<= m , g <=1. The lower line 'L1' represents the boundary between low synchrony and high synchrony. For fitting this line, the points along the border between low

synchrony and high synchrony were obtained. The points were obtained by considering values of ε from 0 to 0.1 in steps of 0.01 and corresponding values of β at which the jump in the value of amplitude synchrony was the most from the previous value of β. The boundary was fit with the relation $\varepsilon = \frac{\kappa}{\beta^{\alpha}}$. 'L1', represents the interpolated line obtained by finding the values of ε for point values of β using the given relation. The mean absolute error of fitting between the actual and predicted values of ε was 0.0013.

The upper line 'L2' represents the boundary which separates points in the parameter space where g>1 and g<=1. This boundary was obtained by fitting all those points in the parameter space that stood at the boundary. For each value of β in the range [0,1] in steps of 0.01, we obtained all those values of ε above which g>1. These points were fit using the relationship $\varepsilon = \frac{\kappa}{\beta^{\alpha}}$. 'L2', represents the interpolated line obtained by finding the values of ε for point values of β using the given relation. The mean absolute error of fitting between the actual and predicted values of ε was 0.0025.

Table II
Results of Fitting the Transition Boundary Lines

Boundary	Curve Fitted	Parameters Obtained	Error of Fitting +/-
Boundary between low synchrony and high synchrony in space of β, ε (L1)	$\varepsilon = \frac{\kappa}{\beta^{\alpha}}$	κ = 0.0132, α = 1.0598	0.0013
Boundary between g>1 and g <=1 (L2)	$\varepsilon = \frac{\kappa}{\beta^{\alpha}}$	κ = 0.0584, α = 0.4081	0.0025

4.2 Coupled CAN oscillators

The principal goal of our research thus far has been to model the behavior of 1000 interacting individual CAN elements under energy/metabolic constraints. The main intention of this effort was to find a set of parameters whereby the energy flow/cycle of each element contributed in the collective of the 1000 elements as a whole to produce robust mesoscopic gamma rhythm oscillations in the network. Indeed, we have achieved this goal in our model/simulations. The end result of this effort is the establishment or construction of what we have referred to as a single "CAN unit." As discussed in Section 1, a CAN unit is a mesoscopic collection of a 1000 CAN elements representing the canonical cortical column or functional unit of cortical operation as it relates to sensori-motor behavior or cognition, be it a human or nonhuman mammalian brain.

The important point to make here is that, while the functional properties of an individual CAN unit are instructive to a discussion on the foundational aspects of energy management in the brain, it is the hierarchical interactions of clusters of millions of these individual CAN units that

give rise to the computational cognitive complexity of human thought and behavior. For example, the posterior sensory cortex of primates/humans is largely dominated by the visual system whereby the columnar organization of what we would call CAN units is instrumental in the formation a visual images there; see Figure 8. Similarly, the auditory and somatosensory cortices are built up from tonotopic and somatotopic maps, respectively, whereby the receptive field mappings there are defined or circumscribed by a columnar architecture.
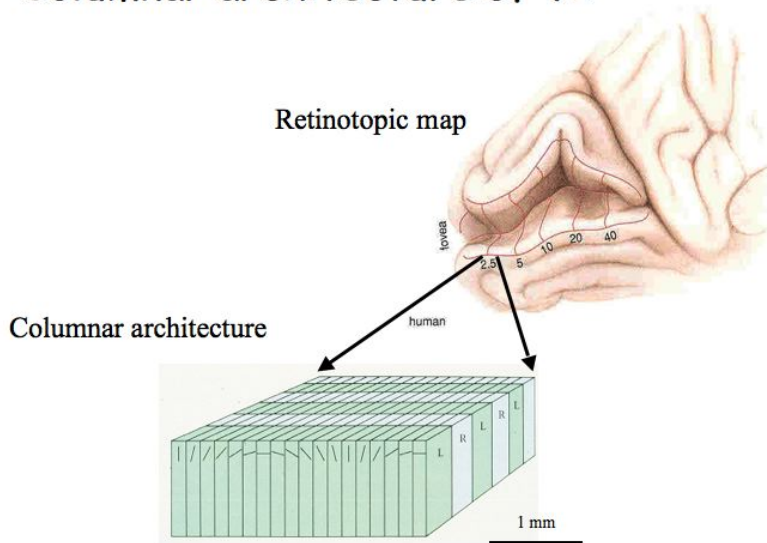

Figure 8: Illustration of columnar organization of primate primary visual cortex, V1, showing orientation and ocular-dominance columns (from http://www.cns.nyu.edu/~david/courses/ perception/lecturenotes/V1/lgn-V1.html).

Not only are the posterior sensory of the cortex organized into a functional columnar structure, so is the frontal motor regions. For example, M1, the primary motor strip, is topographically organized in a rough columnar structure through stimulation mapping. Moreover, certain populations of these functional columnar units in the primate M1 region have been shown to behave in a cooperative fashion, mesoscopically, in the production of ethologically important survival behaviors such as grasping, reaching, and defensive postures (Kaas, 2008); see Fig. 9.
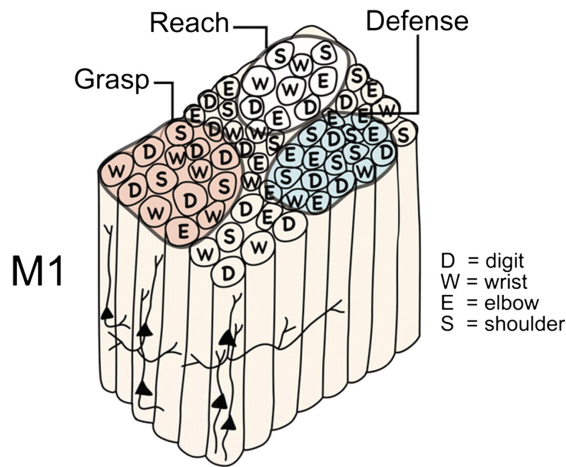
Figure 9: Columnar organization of a section of primate primary motor cortex, M1 (image from http://www.pnas.org/content/109/Supplement_1/10655.full.pdf).

In light of the above findings, we assert that the key to understanding human cognition, behavior, and the energy efficiency in which that brain accomplishes these feats lies in the understanding of the mesoscopic interactions between hierarchical collections or cortical columns. In our model, arrays of the individual CAN units can model such columnar structures.

(a)   (b)
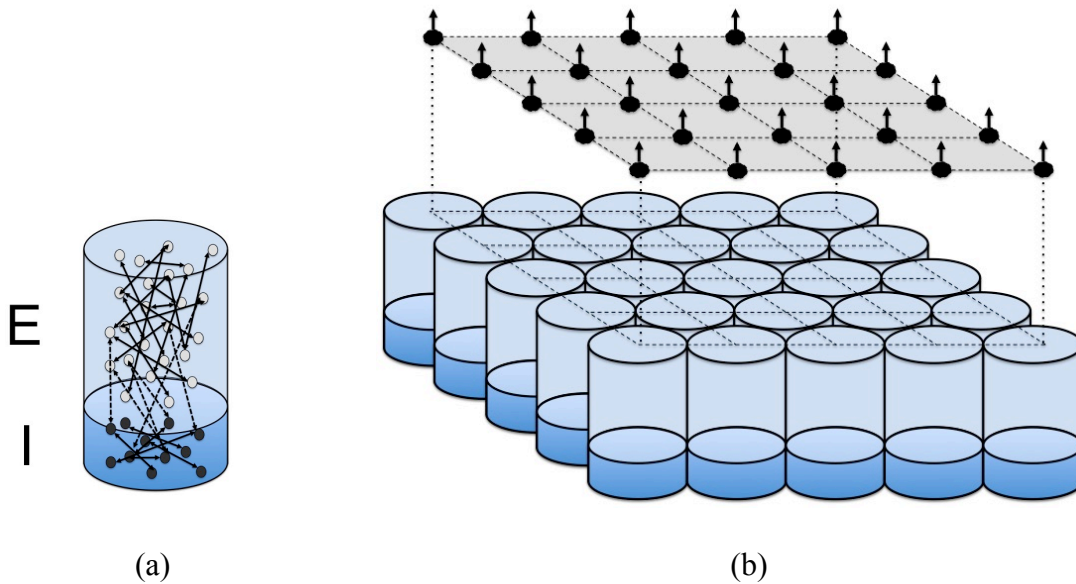
Figure 10. Illustration of the hierarchical organization of the CAN neuro-energetic model; (a) individual CAN populations describing a cortical column with Excitatory and Inhibitory units; (b) array of coupled CAN units modeling interaction cortical columns which execute the computational function using STDP learning rule for the connections between the columns.

A great deal of experimental data on such mesoscopic interactions in the mammalian neocortex has been carried out of the past several decades by some of our team members in collaboration with the late pioneering neuroscientist Walter Freeman. We have a wealth of experimental data to compare out future multi-CAN implementations of the CAN-unit model. Freeman (1991) have identified the formation of spatial amplitude-modulated patterns of neural activity in the rabbit sensory cortex (visual, auditory, olfactory, etc); see Fig. 11. We are excited about our future efforts to extend the CAN unit model into multi-CAN arrays performing machine learning tasks.
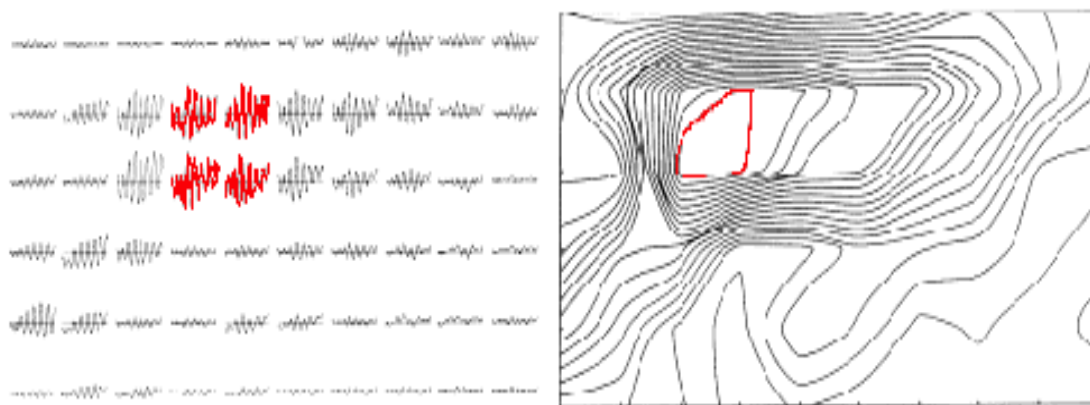

Figure 11: 6x10 micro-array of electrodes implanted on the olfactory cortex of a rabbit (left). Note the commonality of the frequency and phase of each of the 60 EEG recordings on the left. While the frequency and phase of the oscillations are similar across the elements in the array, the amplitudes of each are not. These amplitude-modulated (AM) variations of the potential across the array that give identity and form to cognitive percepts, and that can be visualized as a topographic map (right). In the current formulation, each of the 60 recordings in the above array can be considered an individual CAN unit coupled into a cooperative network. (image from Freeman, 1991).

5. Discussion

In the CAN-unit model, having a similar concentration of ATP in the constitutive neurons or CAN units in cooperatively interacting communities is essential for the requisite synchronous brain rhythms that drive sensory and cognitive processing in those networks. As is revealed in our simulations, the spiking frequency and behavior of neurons is directly affected by the immediate availability or concentration of ATP in the neuron during individual and population spiking "burst" epochs. Therefore, in order to coordinate cooperative activity in these networks, the metabolic cycling of energy precursor molecules must be coordinated between the CAN units that make up the interacting populations.

More specifically, perceptual and cognitive processes in the human brain are accomplished through the formation of what have been referred to as amplitude-modulated (AM) patterns or frames of information in various cortical regions (Freeman, 1991; Kozma and Freeman, 2016). The AM patterns are formed, as described above, through the cooperative or synchronous activity in a collection of CAN units that compose a cytoarchitectonically circumscribed and

defined region of cortex such as the visual cortex (V1) or the motor cortex (M1). Not only are these cognitive perceptual frames coordinated spatially through such synchronization, they are also coordinated temporally through a process referred to as chaotic itinerancy (Freeman 2003: Tsuda 2001). The spatio-temporal coordination of these AM patterns or frames is essential in the formation of perceptions, thoughts, and behaviors in the human nervous system. Disruption of the coordination of these rhythms due to inconsistencies in the energy cycle of the CAN units, such as is witnessed in, say, hypoglycemia or diabetes, lead correspondingly to perceptual-cognitive deficiencies as well as psycho-motor coordination problems (Rosenthal et al., 2001).

6. Conclusions

We have implemented and tested the coupled neurocomputing-metabolic model with explicit energy constraints. The central results are as follows:

1) Our approach demonstrates that the amount of available energy modulates the oscillation frequency of interacting computational units (spiking neurons); more energy inflow (via vascular input) produces increased frequency of oscillations (spiking). Moreover, for a given level of energy supply, we can produce transitions between highly synchronous oscillations (resonances) and desynchronization effects by changing the coupling coefficient from the computational units (neurons) to the metabolic components (astrocytes) acting as a control parameter.

2) In the case of single CAN oscillatory units, we studied the feasible range of parameters maintaining oscillations of energy variables in a stable range, at the same time producing quantifiable variation in the oscillatory frequency (computational capability) as the function of available energy resources. It is also important that the feasible parameters produce high synchrony of oscillations in the single CAN computational unit. We developed the blueprint of coupled CAN oscillator arrays, for the time being 3x3 array, for simplicity.

3) The research conducted in Task 3 of this DARPA project helps to design dynamic regimes with intermittent synchronization regimes in CAN arrays. The demonstrated synchronization control algorithm is a crucial advantage of our approach, as synchronization-desynchronization transitions allow rapid response to dynamically changing external conditions to achieve efficient machine learning and associative memory functions.

The main conclusion to be drawn from the research done in developing the CAN unit model is that the human brain manages its energy stores through 1) coordinating the distribution of energy precursors to cooperatively interacting cortical regions and 2) utilizing the coordinated energy cycles of those cooperating regions to aid in the synchronization of activity between those regions. Coordinating the timing of the dynamics rhythms of dendritic currents allow for an energy efficient means for constructive interference in those networks to sharpen the identity of cognitive-perceptual AM patterns in cortical neuropil with minimal wasted energy being dissipated due to excessive phase dispersion and frequency modulation in the network. While it is unclear whether the lessons learned here will be of any benefit in designing the next generation of traditional, serial-based integrated circuit technology, it will certainly be of great benefit when designing the next generation of massively parallel computing architectures inspired by the computationally impressive and energy efficient human brain.

7. References

Aubert A, Costalat R. (2002) A model of the coupling between brain electrical activity, metabolism, and hemodynamics: application to the interpretation of functional neuroimaging. Neuroimage. 2002 Nov;17(3):1162-81.

Aubert A, Costalat R. (2005) Interaction between astrocytes and neurons studied using a mathematical model of compartmentalized energy metabolism.
J Cereb Blood Flow Metab. 2005 Nov;25(11):1476-90.

Bélanger M, Allaman I, Magistretti PJ. (2011). Brain energy metabolism: focus on astrocyte-neuron metabolic cooperation. *Cell Metabolism* 14(6):724-38

Baldi P., Sadowski P. (2014). The dropout learning algorithm. Artif. Intell. 210, 78–122.

Bandettini PA. (2009) What's new in neuroimaging methods? Ann N Y Acad Sci. 2009 Mar;1156:260-93.

Bandettini P. A. (2012). Twenty years of functional MRI: the science and the stories. Neuroimage62, 575–588.

Brette, R (2015) What Is the Most Realistic Single-Compartment Model of Spike Initiation? PLoS Comput Biol. 2015 Apr; 11(4): e1004114. Energetic constraints produce self-sustained oscillatory dynamics in neuronal networks.

Javier Burroni, P. Taylor, Cassian Corey, Tengiz Vachnadze, Hava T. Siegelmann. Energetic constraints produce self-sustained oscillatory dynamics in neuronal networks.
Front Neurosci. 2017; 11: 80.

Calvetti D, Somersalo E. (2011) Dynamic activation model for a glutamatergic neurovascular
J Theor Biol. 2011 Apr 7;274(1):12-29

Chander BS, Chakravarthy VS. (2012) A computational model of neuro-glio-vascular loop interactions. PLoS One 7(11):e48802.

Chhabria K, Chakravarthy VS. (2016) Low-Dimensional Models of "Neuro-Glio-Vascular Unit" for Describing Neural Dynamics under Normal and Energy-Starved Conditions.
Front Neurol. 2016 Mar 9;7:24

Cloutier, M., Bolger, F.B., Lowry, J.P. and Wellstead, P. 2009. An integrative dynamic model of brain energy metabolism using in vivo neurochemical measurements. *Journal of Computational Neuroscience*, 27(3), pp.391-414.

Filosa JA, Boney AD, Nelson MT (2004) Calcium dynamics in cortical astrocytes and arterioles during neurovascular coupling,. Circulation Research 95: e73–e81

Freeman, WJ. Mass action in the nervous system. 1975. New York: Academic Press.

Freeman, WJ. Evidence from human scalp EEG of global chaotic itinerancy. 2003; *Chaos* 13, 1067-77.

Freeman WJ, Rogers LJ, Holmes MD, Silbergeld DL. (2000) Spatial spectral analysis
of human electrocorticograms including the alpha and gamma bands.
J Neurosci Methods. 2000 Feb 15;95(2):111-21.

Guillery, RW (2005) Observations of synaptic structures: origins of the neuron doctrine and its current status. Philos Trans R Soc Lond B Biol Sci. 2005 Jun 29; 360(1458): 1281–1307

Haueis P. (2016) The life of the cortical column: opening the domain of functional architecture of the cortex (1955-1981). Hist Philos Life Sci. 2016

Holmes MD, Ojemann GA, Lettich E (1996) Neuronal activity in human right lateral temporal cortex related to visuospatial memory and perception. Brain Res. 1996 Mar 4;711(1-2):44-9.

Insel, N Carol A. Barnes (2015) Differential Activation of Fast-Spiking and Regular-
Firing Neuron Populations During Movement and Reward in the Dorsal Medial Frontal Cortex
Cereb Cortex. 2015 Sep; 25(9): 2631–2647.

Izhikevich, E.M., 2003. Simple Model of Spiking Neurons. *IEEE Transactions on Neural Networks*, 14(6), pp.1569-1572.

Izhikevich, E.M. Dynamical systems in neuroscience: The geometry of excitability and bursting. 2007. The MIT press.

Jolivet, R., Coggan, J.S., Allaman, I., Magistretti, P.J., 2015. Multi-timescale modeling of activity-dependent metabolic coupling in the neuron-glia vasculature ensemble. *PLoS Computational Biology*, 11(2), e1004036.

Kaas, JH. Evolution of columns, modules, and domains in the neocortex of primates.
PNAS;109:10655-660.

Kannurpatti SS. (2017) Mitochondrial calcium homeostasis: Implications for neurovascular and neurometabolic coupling. J Cereb Blood Flow Metab. 2017 37(2):381-395.

Kozma, R. and Freeman, W.J., 2016. "Cognitive phase transitions in the cerebral cortex-enhancing the neuron doctrine my modeling neural fields." Springer. New York.

Mangia S, Simpson IA, Vannucci SJ, Carruthers A. (2009) The in vivo neuron-to-astrocyte lactate shuttle in human brain: evidence from modeling of measured lactate levels during visual stimulation. J Neurochem. 2009 May;109 Suppl 1:55-62.

Mason S. (2017) Lactate Shuttles in Neuroenergetics-Homeostasis, Allostasis and Beyond.
Frontiers in Neurosci. 2017 Feb 2;11:43

Mesquita RC, Huppert TJ, Boas DA. (2009) Exploring neuro-vascular and neuro-metabolic coupling in rat somatosensory cortex. Phys Med Biol. 2009 Jan 21;54(2):175-85.

Millet, LJ Martha U. Gillette. Over a Century of Neuron Culture: From the Hanging Drop to Microfluidic Devices. Yale J Biol Med. 2012; 85(4): 501–521.

Moore C. I., Cao R. The hemo-neural hypothesis: on the role of blood flow in information processing. J. Neurophysiol. 2008; 99, 2035–2047.

Moseley ME, Liu C, Rodriguez S, Brosnan T. Advances in magnetic resonance neuroimaging. Neurologic Clinics 2009 Feb;27(1):1-19

Mountcastle V. Modality and topographic properties of single neurons of cat's somatic sensory cortex. Journal of Neurophysiology. 1957;20(4):408–434

Mountcastle V. B. The columnar organization of the neocortex. Brain. 1997 120 (Pt 4):701-22.

Norris D. G. (2006). Principles of magnetic resonance assessment of brain function. J. Magn. Reson. Imaging 23, 794–807.

Ojemann GA, Creutzfeldt O, Lettich E, Haglund MM. (1988) Neuronal activity in human lateral temporal cortex related to short-term verbal memory, naming and reading.
Brain. 1988 Dec;111 (Pt 6):1383-403.

Ojemann JG, Ojemann GA, Lettich E. (1992) Neuronal activity related to faces and matching in human right nondominant temporal cortex. Brain. 1992 Feb;115 Pt 1:1-13.

Philips RT, Chhabria K, Chakravarthy VS. (2016) Vascular Dynamics Aid a Coupled Neurovascular Network Learn Sparse Independent Features: A Computational Model.
Front Neural Circuits. 2016 Feb 26;10:7

Rockland K. S., Ichinohe N. (2004). Some thoughts on cortical minicolumns. Exp. Brain Res. 158, 265–27710

Rockland KS. Five points on columns. Neuroanat. 2010 4:22.

Schneider, DM Sarah M. N. Woolley (2010) Discrimination of Communication Vocalizations by Single Neurons and Groups of Neurons in the Auditory Midbrain, J Neurophysiol. 2010 Jun; 103(6): 3248–3265

SIA (2015) Rebooting the IT Revolution – A Call to Action, Semiconductor Industry Association, September, 2015.

Shibasaki H. (2008) Human brain mapping: hemodynamic response and electrophysiology. Clin Neurophysiol. 2008 Apr;119(4):731-43.

Sickmann HM, Walls AB, Schousboe A, Bouman SD, Waagepetersen HS., 2009 Functional significance of brain glycogen in sustaining glutamatergic neurotransmission. J Neurochemistry109 80-6.

Soares, J M. Ricardo Magalhães, Pedro S. Moreira, Alexandre Sousa, Edward Ganz, Adriana Sampaio, Victor Alves, Paulo Marques, Nuno Sousa (2016) A Hitchhiker's Guide to Functional Magnetic Resonance Imaging. Front Neurosci. 2016; 10: 515.

Srivastava N., Hinton G., Krizhevsky A., Sutskever I., Salakhutdinov R. (2014). Dropout: a simple way to prevent neural networks from overfitting. J. Mach. Learn. Res. 15, 1929–1958.

Tewarie, P, M.G. Bright, A. Hillebrand, S.E. Robson, L.E. Gascoyne, P.G. Morris, J. Meier, P. Van Mieghem, M.J. Brookes (2016) Predicting haemodynamic networks using electrophysiology: The role of non-linear and cross-frequency interactions Neuroimage. 2016 Apr 15; 130: 273–292.

Ts'o DY, Zarella M, Burkitt G. Whither the hypercolumn. Journal of Physiol. 2009; 587(Pt 12):2791-805.

Tsuda, I. Toward an interpretation of dynamic neural activity in terms of chaotic dynamical systems. Behav. Brain Sci. 2001;24:793-847.

Van den Heuvel, M.P. and Hulshoff Pol, H.E., 2010. Exploring the brain network: a review on resting-state fMRI functional connectivity. *European Neuro-psychopharmacology*, 20(8), pp.519-34. Overcoming the blood-brain tumor barrier for effective glioblastoma treatment.

van Tellingen O, Yetkin-Arik B, de Gooijer MC, Wesseling P, Wurdinger T, de Vries HE. Overcoming the blood-brain tumor barrier for effective glioblastoma treatment. Drug Resist Updat. 2015:1-12.

Zonta M, Angulo MC, Gobbo S, Rosengarten B, Hossmann KA, Pozzan T, et al. Neuron-to-astrocyte signaling is central to the dynamic control of brain microcirculation. Nat Neurosci (2002) 6(1):43–50.